COMMUNICATION

Enhanced Power Conversion Efficiency in PCDTBT/$PC_{70}BM$ Bulk Heterojunction Photovoltaic Devices with Embedded Silver Nanoparticle Clusters

Dong Hwan Wang, Keum Hwan Park, Jung Hwa Seo, Jason Seifter, Ji Hye Jeon, Jung Kyu Kim, Jong Hyeok Park, O Ok Park,* and Alan J. Heeger**

Donor-acceptor polymer-fullerene-based bulk heterojunction (BHJ) photovoltaic cells have many advantages; specifically, they can be fabricated in large-areas with simple solution methods involving a low-cost roll-to-roll manufacturing process.[1–7] The active layer in BHJ solar cells provides charge generation, separation, transport, and collection. During these steps, sweep-out of photo-generated carriers competes with charge recombination within the BHJ due to low carrier mobility.[8–10] Blocking the recombination is a key method of increasing device efficiency.[11] Therefore, we need to decrease the thickness of the active layer of BHJ film and maximize its absorption capability to reduce the likelihood of recombination and thereby improve the efficiency of the device.

Metallic silver (Ag) nanoparticles (NPs) can be effective in thin film solar cells because of their localized surface plasmon resonance, which can increase the light absorption capability of an active layer within a range of wavelengths. Thus, the addition of metal NPs into a BHJ active layer can potentially enhance the absorption and increase the photo-generation of mobile carriers. Several groups have recently reported that, when combined, polymer and metal NPs improve light absorption and cell efficiency.[12–15] To ensure that metal NPs have positive effects in organic photovoltaic devices (OPVs), we must diminish the possibility of transferring nonradiative energy, which quenches excitons in the BHJ active layer.[12,15] Because of this concern, most researchers add metal NPs to the interface of the indium tin oxide (ITO) anode and the BHJ active layer; alternatively, they embed the metal NPs in a poly(3,4-ethylene dioxythiophene:poly(styrene sulfonate) (PEDOT:PSS) hole transporting interlayer to induce plasmon excitation within the thin BHJ film.[12,16,17] However, Kim and Carroll directly added Ag or Au NPs to a BHJ polymer and confirmed that the cell efficiency was enhanced by the improved electrical conductivity.[13] The simple method of directly mixing metal NPs in an active layer is attractive because it enhances the overall performance of the cell. Specifically, this method can reduce the device resistance;[13] furthermore, the incident light can be reflected and scattered by the embedded metal NPs while passing through the active layer, thereby increasing the optical path length of the incident light.

Our study demonstrates several positive effects that arise from the addition of Ag NPs with controlled diameter size in BHJ photovoltaic cells fabricated with poly[N-9"-hepta-decanyl-2,7-carbazole-alt-5,5-(4',7'-di-2-thienyl-2',1',3'-benzothiadiazole) (PCDTBT)/ [6,6]-phenyl C_{70} butyric acid methyl-ester ($PC_{70}BM$). Using effective, easily processable solution chemistry of a polyol process, we can synthesize Ag particles with well-controlled sizes and well-defined shapes. Specifically, we produced particles with diameters of 30 nm, 40 nm, and 60 nm. These Ag NPs have different absorption spectra. To investigate the photovoltaic device performance, we blended the Ag NPs into a BHJ solution with weight ratios varying from 0.2 wt% to 2 wt%. Ag clusters are formed by the aggregated NPs during the spin coating process. At an optimized blend ratio of 1 wt% with the 40 nm-sized NPs based Ag clusters in PCDTBT/$PC_{70}BM$, the power conversion efficiency increased from 6.3% to 7.1%. Because aggregated large-sized nanomaterials can reflect and scatter incident light more efficiently than small Ag NPs (of less than 10 nm), light can be harvested more effectively.[14] In this study, we discuss how photovoltaic devices perform when the Ag clusters from aggregated NPs with different diameter size are added into the BHJ film.

Figure 1 shows the proposed device structure and the chemical structures of PCDTBT and $PC_{70}BM$. It also shows the scanning electron microscopy (SEM) images of synthesized Ag NPs with different diameters of 30 nm, 40 nm, and 60 nm. These

D. H. Wang, J. Seifter, Prof. A. J. Heeger
Center for Polymers and Organic Solids
University of California
Santa Barbara, California, 93106, USA
E-mail: ajhe@physics.ucsb.edu
D. H. Wang, K. H. Park, J. H. Jeon, Prof. O O. Park
Department of Chemical and Biomolecular Engineering
Korea Advanced Institute of Science and Technology
(BK 21 Graduate Program)
373-1 Guseong-dong, Yuseong-gu, Daejeon 305-701, Republic of Korea
E-mail: ookpark@kaist.ac.kr
Prof. J. H. Seo
Department of materials physics
college of natural science
Dong-A University
840 Hadan2dong, Sahagu, Busan 604-714, Republic of Korea
J. K. Kim, Prof. J. H. Park
Department of Chemical Engineering
Sungkyunkwan University
Suwon 440-746, Republic of Korea
E-mail: lutts@skku.edu
Prof. O O. Park
Department of Energy Systems Engineering
Daegu Gyeongbuk Institute of Science and Technology (DGIST)
50-1, Sang-ri, Hyeongpung-myeon, Dalseong-gun, Daegu 711-873
Republic of Korea

DOI: 10.1002/aenm.201100347

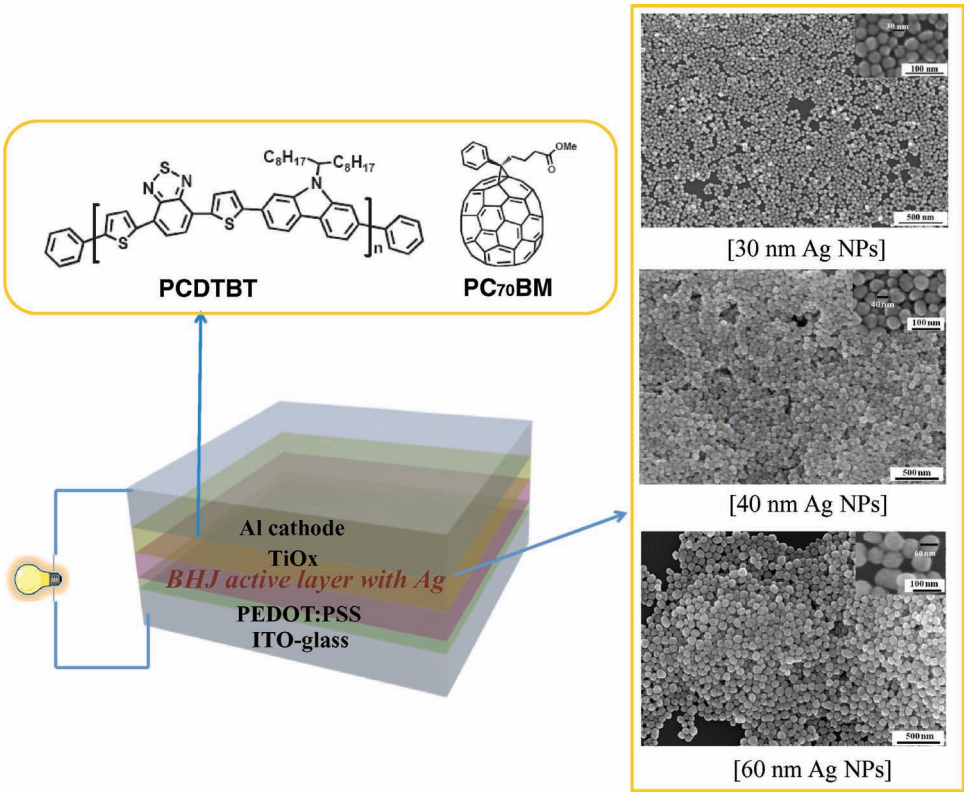

Figure 1. Chemical structures of PCDTBT and $PC_{70}BM$; a schematic of the device structure; and SEM images of synthesized Ag NPs of several diameters (30 nm, 40 nm, and 60 nm) using polyol process.

synthesized Ag NPs have a uniformly controlled shape and size. As revealed by the results of energy dispersive spectroscopy (EDS) in Figure S1, the synthesized NPs are composed of elemental Ag. These Ag NPs are a good material for investigating the size effects of Ag in OPVs. Typical polyol chemistry is used to synthesize Ag NPs. Specifically, silver nitrate ($AgNO_3$) (Aldrich) is used as a precursor of silver, and poly-(vinylpyrrolidone) (PVP) (Aldrich, Molecular weight (Mw) = 55,000) is used as a surfactant for Ag salt. Ag atoms can then be obtained by reducing $AgNO_3$ with 1,2-Propanediol (PrD: Sigma Aldrich) in the presence of deionized water through the following reaction:[18–22]

$$HOC_4H_8OH + 1/2O_2 \rightarrow HOC_3H_6CHO + H_2O$$

$$2Ag^+ + HOC_3H_6CHO + H_2O \rightarrow 2A\,g + HOC_3H_6COOH + 2H^+$$

The size and shape of synthesized Ag NPs vary in relation to the control of the solution mixture concentration, the solvent, the reaction time, and the reaction temperature.[23]

Figure 2(a) shows ultraviolet (UV)-visible absorption spectra of synthesized Ag NPs with different diameters dispersed in ethanol. Thus, the 30 nm, 40 nm, and 60 nm Ag NPs have a maximum absorbance near 390 nm, 420 nm, and 450 nm, respectively. The synthesized Ag NPs with a 60 nm diameter have a much broader absorption peak when well dispersed in solution. Figure 2(b) shows increased absorption by the 40 nm-sized NPs based Ag clusters embedded in the BHJ film (1 wt%); the improved absorption originates in the light scattering of the Ag clusters.[12] The inset of Figure 2(b) shows a schematic of the light trapping and optical reflection caused by the scattering from the Ag clusters in the BHJ. The Ag clusters increase the effective optical path length by means of scattering and the generation of electron-hole pairs from the surrounding excited fields of the Ag clusters. A BHJ film with Ag clusters has superior absorption because it can scatter the incident light through a whole range of wavelengths (in the transmittance mode of the UV-visible absorption equipment, the light scattering resembles the absorption shown in Figure 2 and S2.) Therefore, the PCDTBT/$PC_{70}BM$ BHJ films with 40 nm-sized NPs based Ag clusters (1 wt%) have greater optical absorbance than a plain PCDTBT/$PC_{70}BM$ BHJ at around 350 nm to 550 nm.

Figure 3(a) to 3(d) show atomic force microscopy (AFM) and scanning electron microscopy (SEM) images of the plain PCDTBT/$PC_{70}BM$ BHJ, and the BHJ with the 40 nm-sized NPs based Ag clusters (1 wt%). The individual Ag NPs aggregate during the film casting. Therefore, randomly distributed Ag clusters are formed on the top of the polymer-based active layer films. The SEM image of Figure 3(c) also reveals that the Ag clusters from NPs are randomly dispersed on the top surface of active layer. The SEM high resolution image of Figure 3(d) shows that the Ag clusters are composed of aggregated NPs with well-defined size.

Figure 4(a) shows the photocurrent-voltage curves of a plain BHJ (PCDTBT/$PC_{70}BM$) device and BHJ devices embedded

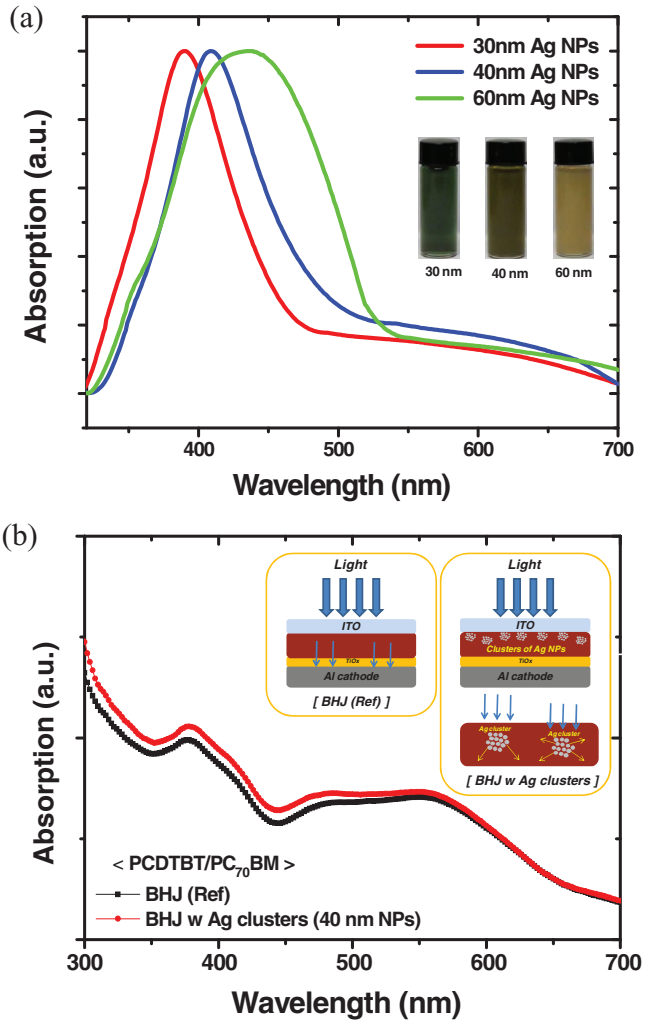

Figure 2. UV visible spectra of (a) Ag NPs of several diameters (30 nm, 40 nm, and 60 nm); (the inset figure shows Ag NPs of different colors dispersed in an ethanol) (b) the plain PCDTBT/PC_{70}BM BHJ film and the BHJ film with 40 nm-sized NPs based Ag clusters (1 wt%). The inset schematic figures show the light trapping and optical reflection by the scattering and excitation of localized surface plasmons.

with Ag clusters with several diameters of 30 nm, 40 nm, and 60 nm and a 1 wt% ratio of donor-acceptor polymers. The plain PCDTBT/PC_{70}BM BHJ device has a power conversion efficiency of 6.3%, an open-circuit voltage (V_{oc}) of 0.86 V, a short-circuit current (J_{sc}) of 10.79 mA/cm^2, and a fill factor (*FF*) of 0.68. The BHJ devices that have optimized 1 wt% Ag clusters with the diameters of 30 nm, 40 nm, and 60 nm Ag NPs have improved power conversion efficiency (PCE) values of 7.0%, 7.1%, and 6.7%, respectively. The critical factors that increase the efficiency of the device are J_{sc} (increased from 10.79 mA/cm^2 to 11.61 mA/cm^2 and *FF* (increased from 0.68 to 0.69) in 40 nm-sized NPs based Ag clusters embedded BHJ film (1 wt%). The inset Figure 4(a) indicates that the series resistance is reduced from 1.62 Ωcm^2 (without Ag clusters) to 1.37 Ωcm^2 (with Ag clusters), consistent with improved charge transport and higher short circuit currents. The ratio of the polymer-based active layer and the Ag clusters were optimized by varying the

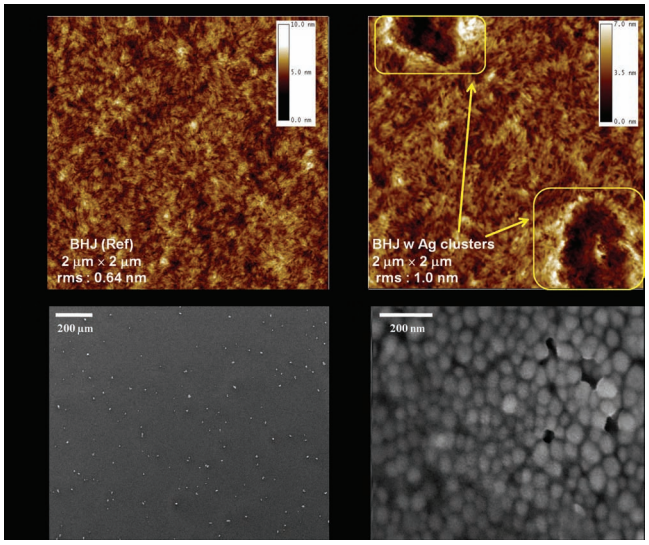

Figure 3. AFM images of the active layer of (a) the plain PCDTBT/PC_{70}BM BHJ, (b) the BHJ with 40 nm-sized NPs based Ag clusters (1 wt%), SEM (c) low and (d) high resolution images of the BHJ with Ag clusters (1 wt%).

concentration from 0.2 wt% to 2 wt%. If the BHJ active layer is blended with Ag clusters at a ratio of 2 wt%, the J_{sc} value is similar with that of the plain BHJ device, but a decreased V_{oc} and a reduced *FF* were obtained as shown in Figure S3. Figure S4 shows the values of the PCE, V_{oc}, J_{sc}, and *FF* for the plain PCDTBT/PC_{70}BM BHJ and the BHJ device made of Ag clusters (1 wt%) as a function of the active layer with a thickness range of 80 nm to 180 nm. In terms of improved cell performance, all the BHJ devices embedded with Ag clusters outperform the BHJ devices of various film thicknesses.

To find the reason for the improved J_{sc}, we measured the incident photon-to-current efficiency spectra for the plain BHJ device and the device with 40 nm-sized NPs based Ag clusters in the BHJ film (1 wt%). The inset of Figure 4(b) shows that for the device with the Ag clusters, the external quantum efficiency (EQE) exceeds 75% near 450 nm. Moreover, as shown in Figure 4(b), EQE enhancement is observed in the wavelength range of 350 nm to 550 nm for the BHJ active layer blended with Ag clusters of an optimized weight ratio and size. The EQE improvements can be attributed to the effect of the Ag clusters in the devices.[24]

Ultraviolet photoelectron spectroscopy (UPS) was used to probe the energy level difference between the plain BHJ and BHJ with Ag clusters. Figure 4(c) shows the UPS results for the plain PCDTBT/PC_{70}BM film (black) and the BHJ film (red) with the Ag clusters; the bare PEDOT:PSS/ITO is the reference. An examination of the secondary electron cutoff (E_{SE}) region in Figure 4(c) and 4(d) (in the range of 15 eV to 17 eV) enables the shift in the vacuum level (E_{vac}) to be extracted.[25,26] The Ag-added BHJ layers produce a shift toward higher binding energies. The E_{vac} shift denotes the magnitude of the interfacial dipole (Δ). The highest occupied molecular orbital (HOMO) energy levels (E_{HOMO}) were determined from the low binding energy region (0 eV to 3 eV). The energy difference between E_{HOMO} and the zero binding energy, as shown in Figure 4(d),

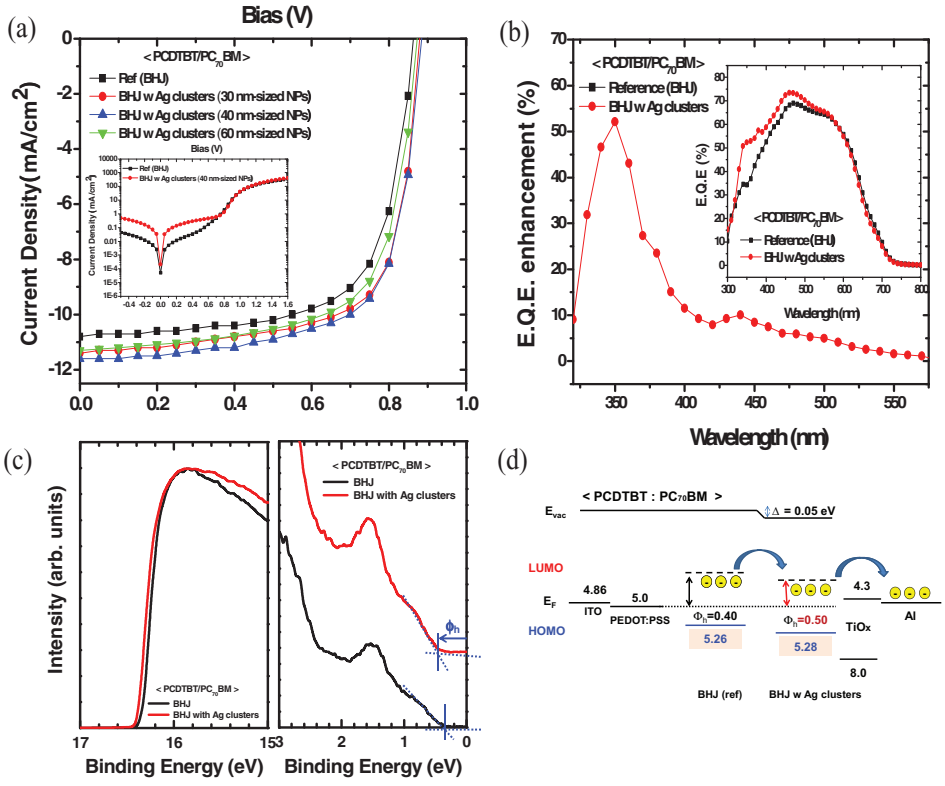

Figure 4. (a) The *J-V* curves of devices with the plain PCDTBT/$PC_{70}BM$ BHJ and the BHJ with Ag clusters from a ratio of 1 wt% and several NPs diameters (30 nm, 40 nm, and 60 nm). The inset figure shows *J–V* curves of the devices with the plain PCDTBT/$PC_{70}BM$ BHJ and the BHJ with the 40 nm-sized NPs based Ag clusters (1 wt%) in the dark current (b) EQE enhancement spectra of the devices from BHJ with 40 nm-sized NPs based Ag clusters (1 wt%). The inset figure shows measured EQE of the plain BHJ and the BHJ with Ag clusters. (c) UPS spectra d) energy diagrams of the plain BHJ (black) and the BHJ with Ag clusters (1 wt%) (red). (E_{vac}: vacuum level; E_F: Fermi level; Δ: interfacial dipole; Φ_h: hole injection barrier).

corresponds to the hole injection barrier (Φ_h) in optoelectronic devices. The Φ_h for PCDTBT/$PC_{70}BM$ is 0.40 eV relative to the work function of PEDOT:PSS/ITO. From Figure 4(d), we can also estimate that the introduction of Ag clusters increases Φ_h to 0.50 eV. Because Ag clusters are located in the active layer near the cathode (Figure 3(c) and 3(d)), the Ag clusters are likely to affect the charge transport from the BHJ to the cathode, resulting in improved J_{SC} and FF. Assumed the energy gap is not changed, the downward shift of vacuum level causes an increased hole injection barrier, leading to a smaller electron transport barrier.

In conclusion, we have demonstrated the positive effects of Ag clusters composed of Ag NPs in PCDTBT/$PC_{70}BM$ BHJ-based photovoltaic devices. The Ag NPs are synthesized to have several different diameters by using solution polyol chemistry through the control of reactant and reaction conditions. The Ag clusters from NPs are formed by aggregation of NPs during film casting in the BHJ. The Ag clusters (from NPs) improve the values of V_{oc}, J_{sc}, *FF*, and the EQE. These results are due to enhanced light absorption. The improved charge transport also increases the value of J_{sc} and reduces the resistance. Finally, from 1 wt% and the 40 nm-sized NPs based Ag clusters embedded BHJ active layer, the power conversion efficiency of the device can be increased from 6.3% to 7.1%.

Experimental Section

Synthesis of Ag NPs: In a typical synthesis, 3.0 mL of a 94 mM sample of $AgNO_3$, 3.0 mL of a 147 mM sample of poly-(vinylpyrrolidone), and 6 mL of polyol are mixed and heated at 140 °C for 1 h. We use $AgNO_3$ (Aldrich) as the precursor of the Ag NPs and PVP (Aldrich, Mw = 55 000) as the surfactant. To control the size of the Ag NPs, we use three kinds of polyols: 1,2-propanediol (PrD: Sigma Aldrich), 1,4-butanediol (BD: Sigma Aldrich), and 1,5-Pentanediol (PtD: Aldrich). The smaller NPs are synthesized in a more viscous medium. The polyol viscosity increases as the hydrocarbon chain is elongated in the order of PrD < BD < PtD. The size of the synthesized NPs decreases in the order of PrD (60 nm) > BD (40 nm) > PtD (30 nm). The synthesized silver NPs are collected by means of centrifugation with the addition of water and ethanol.

Device fabrication: Photovoltaic devices based on PCDTBT/$PC_{70}BM$ with a blend of Ag clusters from NPs are prepared as shown in Figure 1. The impurities are removed from the ITO glass through a cleaning process. We subject the ITO glass to UV treatment for 15 min to reform the ITO surface before spin-casting a 35 nm layer of PEDOT:PSS (Baytron PH) on top of the ITO and then baked at 140 °C for 10 min. On top of the PEDOT/PSS layer, we spin-coat about an 80 nm layer of BHJ made with Ag NPs at weight ratios of 0.2 wt%, 1 wt%, and 2 wt% in a mixed solution of PCDTBT/$PC_{70}BM$ (7 mg:28 mg = 1:4) in 1,2-dichloro benzene:chlorobenzene (3:1). The films are dried at 80 °C for 10 min in the glove box. The TiO_x interlayer is then spin-coated to a thickness of approximately 10 nm (5000 rpm, 40 s) in air,[10] and an Al metal cathode is deposited by a thermal evaporator to a thickness of 100 nm under a pressure of 4.0×10^{-6} Torr. The performances of the devices were measured with an Air Mass 1.5 Global (AM 1.5 G) solar simulator at an

intensity of 1000 W m^{-2}. A Keithley 236 source measure unit was used to measure the current density-voltage characteristics of the devices. An aperture with an area of 9.84 mm^2 was used on top of the cell to confirm the accuracy of the device area. The surface morphology was observed with an atomic force microscope (Veeco, USA; D3100) and a scanning electron microscope (FEI Sirion XL 30).

Supporting Information

Supporting Information is available from the Wiley Online Library or from the author.

Acknowledgements

This work was supported by a grant from the ERC program (R11-2007-045-01002-0(2009)) and the WCU program (R32-2008-000-10142-0) through the NRF of Korea funded by the MEST. Research at UCSB was supported by the US Army General Technical Services (LLC/GTS-S-09-1-196) and by the Department of Energy (BES-DOE- ER46535). This research was supported by Future-based Technology Development Program (Nano Fields) through the NRF funded by the MEST (2010-0029321). This work was supported by the National Research Foundation of Korea Grant funded by the Korean Government (MEST) (NRF-2009-C1AAA001-2009-0094157, 2009-0083540).

Received: June 23, 2011
Published online: August 22, 2011

[1] G. Yu, J. Gao, J. C. Hummelen, F. Wudl, A. J. Heeger, *Science* **1995**, *270*, **1789**.
[2] A. J. Heeger, *Angew. Chem. Int. Ed.* **2001**, *40*, 2591.
[3] J. Peet, M. L. Senatore, A. J. Heeger, *Adv. Mater.* **2009**, *21*, 1521.
[4] W. Ma, C. Yang, X. Gong, K. H. Lee, A. J. Heeger, *Adv. Funct. Mater.* **2005**, *15*, 1617.
[5] G. Dennler, M. C. Scharber, C. J. Brabec, *Adv. Mater.* **2009**, *21*, 1323.
[6] D. H. Wang, D. G. Choi, O. O. Park, J. H. Park, *J. Mater. Chem.* **2010**, *20*, 4910.
[7] D. H. Wang, J. S. Moon, J. Seifter, J. Jo, J. H. Park, O O. Park, A. J. Heeger, *Nano Lett.*, [Online early access]. doi.org/10.1021/nl202320r.
[8] P. W. M. Blom, V. D. Mihailetchi, L. J. A. Koster, D. E. Markov, *Adv. Mater.* **2007**, *19*, 1551.
[9] D. E. Markov, E. Amsterdam, P. W. M. Blom, A. B. Sieval, J. C. Hummelen, *J. Phys. Chem. A* **2005**, *109*, 5266.
[10] D. H. Wang, S. H. Im, H. K. Lee, J. H. Park, O. O. Park, *J. Phys. Chem. C*, **2009**, *113*, 17286.
[11] S. H. Park, A. Roy, S. Beaupré, S. Cho, N. Coates, J. S. Moon, D. Moses, M. Leclerc, K. Lee, A. J. Heeger, *Nat. Photon.* **2009**, *3*, 297.
[12] H. A. Atwater, A. Polman, *Nat. Mater.* **2010**, *9*, 205.
[13] K. Kim, D. L. Carroll, *Appl. Phys. Lett.* **2005**, *87*, 203113.
[14] D. H. Wang, D. Y. Kim, K. W. Choi, J. H. Seo, S. H. Im, J. H. Park, O O. Park, A. J. Heeger, *Angew. Chem. Int. Ed.* **2011**, *50*, 5519.
[15] C.-H. Kim, S.-H. Cha, S. C. Kim, M. Song, J. Lee, W. Shin, S.-J. Moon, J. H. Bahng, N. A. Kotov, S.-H Jin, *ACS Nano* 2011, 5, 3319.
[16] J. H. Lee, J. H. Park, J. S. Kim, D. Y. Lee, K. Cho, *Org. Electron.* **2009**, *10*, 416.
[17] R. B. Konda, R. Mundle, H. Mustafa, O. Bamiduro, A. K. Pradhan, U. N. Roy, Y. Cui, A. Burger, *Appl. Phys. Lett.* **2007**, *91*, 191111.
[18] Y. Sun, Y. Xia, *Adv. Mater.* **2002**, *14*, 833.
[19] K. H. Park, S. H. Im, O O. Park, *Nanotechnology* **2011**, *22*, 045602.
[20] R. Jin, Y. Cao, E. Hao, G. S. Métraux, G. C. Schatz, C. A. Mirkin, *Nature* **2003**, *425*, 487.
[21] V. F. Puntes, K. M. Krishnan, A. P. Alivisatos, *Science* **2001**, *291*, 2115.
[22] Y. Xia, P. Yang, Y. Sun, Y. Wu, B. Mayers, B. Gates, Y. Yin, F. Kim, H. Yan, *Adv. Mater.* **2003**, *15*, 353.
[23] Y. Sun, B. Mayers, T. Herricks, Y. Xia, *Nano Lett.* **2003**, *3*, 955.
[24] M. G. Kang, T. Xu, H. J. Park, X. Luo, L. J. Guo, *Adv. Mater.* **2010**, *22*, 4378.
[25] S. Braun, W. R. Salaneck, M. Fahlman, *Adv. Mater.* **2009**, *21*, 1450.
[26] J. H. Seo, R. Yang, J. Z. Brzezinski, B. Walker, G. C. Bazan, T.-Q. Nguyen, *Adv. Mater.* **2009**, *21*, 1006.